DOI: https://doi.org/10.37434/tpwj2024.02.02

INFLUENCE OF PREHEATING ON TIG WELDING THERMAL CYCLE OF HIGH-TEMPERATURE TITANIUM ALLOY OF Ti–Al–Zr–Sn–Mo–Nb–Si SYSTEM

R.V. Selin[1], **V.Yu. Bilous**[1], **S.B. Rukhanskyi**[1], **I.B. Selina**[2], **L.M. Radchenko**[1]

[1]E.O. Paton Electric Welding Institute of the NASU
11 Kazymyr Malevych Str., 03150, Kyiv, Ukraine
[2]National Technical University of Ukraine "Igor Sikorsky Kyiv Polytechnic Institute"
37 Prospect Beresteiskyi (former Peremohy), 03056, Kyiv, Ukraine

ABSTRACT

The main direction of improving the operational characteristics of titanium alloys is creation of heat-resistant and high-temperature titanium alloys. The high specific strength and corrosion resistance of this type of alloys at temperatures up to 500–600 °C, enables making them the main structural material for aircraft and rocket engineering. However, their widespread use is associated with the problem of precipitation of brittle phases during welding, which requires additional technological operations, such as local heat treatment or preheating. In this paper, the finite element modeling method was applied to study the influence of the TIG welding thermal cycle of high-temperature titanium alloy of Ti–6.5Al–5.3Zr–2.2Sn–0.6Mo–0.5Nb–0.75Si system with and without the use of preheating and to plot the cooling rate diagrams of the produced welded joints.

KEYWORDS: high-temperature titanium alloy, TIG welding, finite element modeling, preheating

INTRODUCTION

Owing to a unique combination of physical and mechanical characteristics, titanium alloys are one of the most promising structural materials. Continuous expansion of production and application of titanium in different technology fields is due, first of all, to its higher specific strength (ratio of ultimate strength to density). Excellent corrosion resistance of titanium under atmospheric conditions, in sea water and other environments determines its effective application for fabrication of various structures [1]. The main direction of further improvement of mechanical and service properties of titanium alloys is creation of new generation high-temperature titanium alloys, doped by refractory elements, such as niobium. High specific strength and corrosion resistance of alloys of this type at up to 500–600 °C temperatures allows making them the main structural material for aircraft and rocket engineering. Their wide application, however, is related to poor weldability, which requires taking additional technological measures, such as pre- or concurrent heating and postweld heat treatment. Application of mathematical modeling of the welding thermal cycle allows establishing the cooling rate distribution, determination of the structural-phase state of metal of the weld and HAZ, optimizing the conditions of phase transformation occurrence due to application of welding modes with higher values of energy input or use of preheating, in order to form the state required for achieving higher mechanical properties of welded joints, and possible improvement of welding operation productivity [2].

Table 1. Chemical composition of the high-temperature titanium alloy

Ti	Al	Zr	Sn	Mo	Nb	Si
Base	6.5	5.3	2.2	0.6	0.5	0.75

OBJECTIVE OF THE WORK

is to study the peculiarities of the influence of thermal cycle of tungsten electrode argon-arc (TIG) welding with preheating on the shape and size of the penetration zone and HAZ, as well as distribution of cooling rates in the metal of the weld and HAZ.

INVESTIGATION MATERIALS AND METHODS

Investigation of the influence of thermal cycle of TIG welding with preheating was conducted for high-temperature titanium alloy, the chemical composition of which is given in Table 1 [3, 4].

Computational study of the influence of welding thermal cycle on the structural-phase state of welded joints on two-phase titanium alloys was performed using a nonstationary thermal finite element analysis, taking into account the heat of phase transition. Mathematical modeling of TIG welding was performed by finite element method. A 3D mathematical model of thermal processes in titanium in welding with

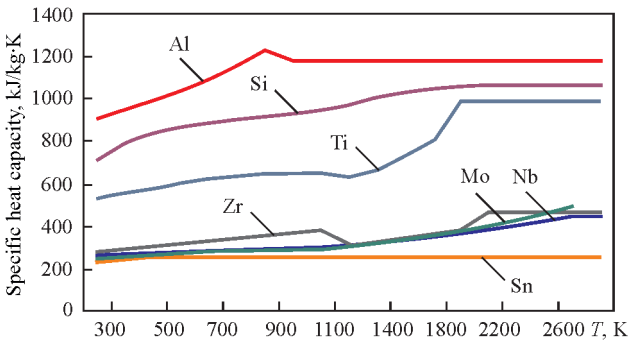

Figure 1. Heat capacity of alloying elements of high-temperature titanium alloy Ti–6.5Al–5.3Zr–2.2Sn–0.6Mo–0.5Nb–0.75Si

a moving heat source was constructed. To perform nonstationary thermal analysis with phase transition, it is necessary to determine the enthalpy dependence on temperature for high-temperature alloy Ti–6.5Al–5.3Zr–2.2Sn–0.6Mo–0.5Nb–0.75Si [5, 6]. Among the numerous empirical relationships of solids, proposed for calculation of heat capacities, the most widespread is the Neumann–Kopp rule, also known as the rule of heat capacity additivity [7]. It allows approximate calculation of chemical compound heat capacity. In keeping with this rule, the molar heat capacity of chemical compounds in the solid state is equal to the sum of molar heat capacities of elements included into this compound. A relationship of the following type is used for an approximate evaluation of specific heat capacity of the alloy [7]:

$$C = pC_1 + qC_2 + \ldots, \quad (1),$$

where C is the specific heat capacity of the alloy; p, q are the weight fractions of the alloy components; C_1, C_2 are the specific heat capacities of the alloy components.

Heat capacities of alloying elements are given in the graph (Figure 1). The given formula (1) was used to establish the temperature dependence of enthalpy for the experimental high-temperature titanium alloy Ti–6.5Al–5.3Zr–2.2Sn–0.6Mo–0.5Nb–0.75Si, compared to heat capacity of VT1-00 titanium alloy (Figure 2).

Heat capacity at 0 °C temperature is equal to 0.526 (kJ/kg·K). In the temperature range from 327 up to 1127 K, the heat capacity of alloy Ti–6.5Al–5.3Zr–2.2Sn–0.6Mo–0.5Nb–0.75Si is approximately 5–7 % higher than that of VT1-00 alloy, and in the temperature range from 1527 to 1860 K it is by 7–10 % lower.

During investigations the influence of such TIG process parameters as welding current, arc voltage, speed of anode spot movement on the dimensions and shape of base metal penetration and HAZ, and probable phase composition of the metal of the weld and HAZ was taken into account.

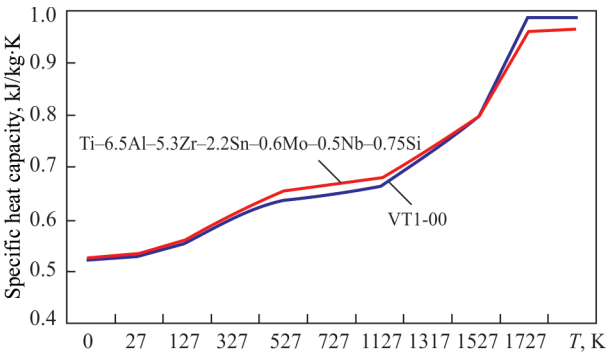

Figure 2. Heat capacity of high-temperature titanium alloy Ti–6.5Al–5.3Zr–2.2Sn–0.6Mo–0.5Nb–0.75Si

Modeling was performed for plates of 200×600×6 mm dimensions. A computational finite element additive grid with sizes shown in Figure 3 was applied to the model constructed by these dimensions.

A 3D mathematical model of thermal processes in titanium during welding was plotted for computational determination of the influence of welding mode parameters on weld formation, taking into account the above assumptions. The model is based on the following differential equation of heat conductivity [9, 10]:

$$\rho c\left(\frac{\delta T}{\delta t}\right) = \frac{d}{dx}\left(\lambda_x \frac{dT}{dx}\right) + \frac{d}{dy}\left(\lambda_y \frac{dT}{dy}\right) + \frac{d}{dz}\left(\lambda_z \frac{dT}{dz}\right), \quad (2)$$

where t is the current time, s; ρ is the material density, kg/m^3; c is the specific heat conductivity, kJ(kg·K); λ is the coefficient of heat conductivity, W/(m·K).

Boundary conditions were formulated, which describe the sample heat exchange with the environment, as well as the welding heat source. In the general case, the following initial and boundary conditions were determined:

1. $T_{t=0} = T_{am}$ is the specified product temperature at the initial moment of time, which is equal to ambient temperature (20 °C).

2. The heat flow on the surface in the zone of impact of the welding heat source is equal to:

$$-\lambda \frac{\partial T}{\partial t} = q_T + q_n + q_s, \quad (3)$$

where q_n is the convective heat exchange, W/(m^2·K):

$$q_T = h_f (T - T_{am}), \quad (4)$$

where h_f is the coefficient of convective heat transfer; in this model it is believed to be constant and equal to 70 W/(m^2·K), T_{am} is the ambient temperature; T is

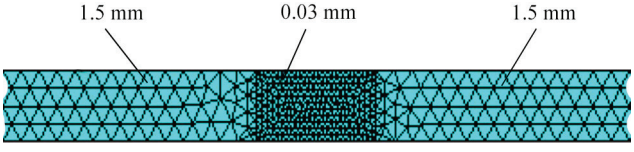

Figure 3. Finite element adaptive grid used for computations

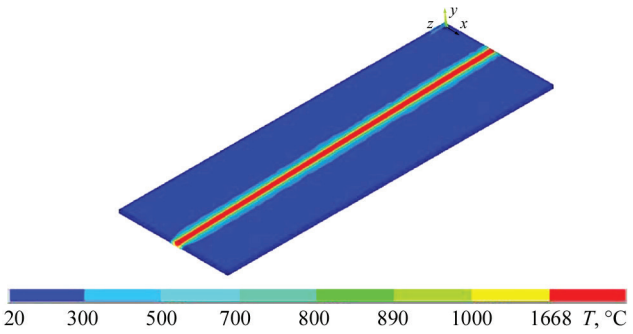

Figure 4. Distribution of maximal temperatures in the welded joint after argon-arc welding simulation

the model surface temperature; q_n is the radiation heat transfer, W/(m²·K):

$$q_n = \varepsilon\sigma\left(T^4 - T_{am}^4\right), \quad (5)$$

where ε is the radiation coefficient, equal to 0.3; σ is the Stephan–Boltzmann constant (σ = 5.6704·10⁻⁸ W/(m⁻²·K⁻⁴); q_s is the distribution of the heat flux from the heat source, W/(m⁻²·K):

$$q_s = q_m \exp\left\{-\frac{(x-Vt)^2 + y^2}{R^2}\right\}, \quad (6)$$

where q_m is the largest heat flow in the heating center, W/(m²·K), V is the welding speed, m/s, R is the radius of the heating spot, m.

Thermal field calculation was performed for 3 welding modes (Table 2). Mode 1 envisages producing a welded joint with incomplete penetration and without preheating, mode 2 is the same, as mode 1, but with preheating to produce complete penetration; mode 3 ensures the same penetration depth, as in mode 1, but with lower energy input and preheating (Mode 3).

INVESTIGATION RESULTS

Thermal fields in the welded product were calculated taking into account the abovementioned initial and boundary conditions. Calculation results were the base to plot the isotherms of maximal temperatures, which were used to determine the geometry and dimensions of the penetration zone, HAZ, and polymorphous transformation zone. Figure 4 shows the result

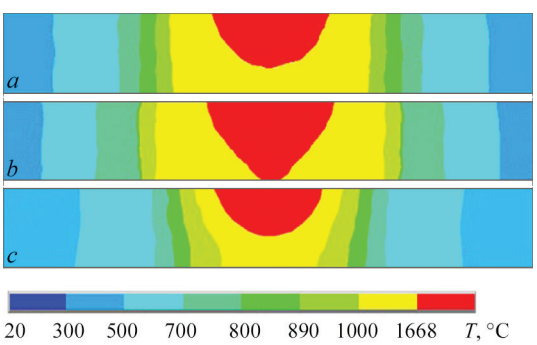

Figure 5. Shape and dimensions of penetration zone (weld metal) and HAZ: *a* — mode 1; *b* — mode 2; *c* — mode 3

Table 2. Modes of argon-arc welding of high-temperature titanium alloy Ti–6.5Al–5.3Zr–2.2Sn–0.6Mo–0.5Nb–0.75Si

Mode No.	Welding current, A	Arc voltage, V	Welding speed, m/h	Preheating, °C
1	310	12	8	–
2	310	12	8	400
3	190	12	8	400

of thermal field calculation in the welded joint in the 3D format.

Such welding modes were selected, at which complete and incomplete penetration of the weld metal can be achieved. This was done in order to determine the influence of preheating on the shape and dimensions of the metal of the weld and HAZ. No complete penetration was achieved in mode 1 (Figure 5, *a*). Penetration depth is 4.2 mm, deposited bead width — 9.2 mm, area — 28.5 mm², HAZ width is equal to 13 mm, area — 73 mm². The same depth, width and area were produced in mode 3 (Figure 5, *c*).

In mode 2 (Figure 5, *b*) the penetration zone width is equal to 10. 8 mm (by 17 % larger than in mode 1), area is 56 mm² (by 96 % larger than in mode 1). HAZ width in this mode is equal to 18.05 mm, and area is 107 mm².

Comparison of calculation results with experimental data confirmed the adequacy of the developed mathematical model (Figure 6). The difference in the penetration zone width in the calculated and experimental sample was 4 %, and for the reverse bead width it was 3 %.

Graphs of the welding thermal cycle for all the modes were plotted in four points: point 1 – on the surface in the weld middle, point 2 — in the weld middle at 3 mm distance from the surface; point 3 — on the HAZ surface at 14 mm distance from the weld middle, point 4 — in the HAZ at 3 mm distance from the surface and 14 mm distance from the weld middle.

One can see from the plotted graphs that in the weld metal the fastest to cool is the metal in mode 1. Preheating application allowed lowering the cooling rates of the samples (Figure 7).

Experimental thermal cycles of TIG welding were obtained to confirm the calculations. TIG welding of high-temperature titanium alloy Ti–6.5Al–5.3Zr–2.2

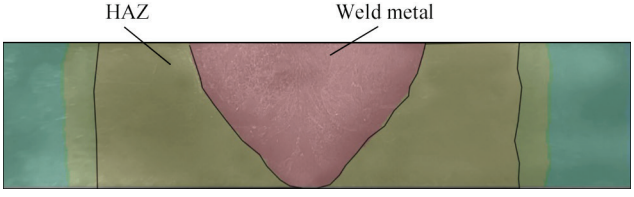

Figure 6. Verification of model adequacy using a macrosection of the welded joint of high-temperature titanium alloy Ti–6.5Al–5.3Zr–2.2Sn–0.6Mo–0.5Nb–0.75Si made in mode 2

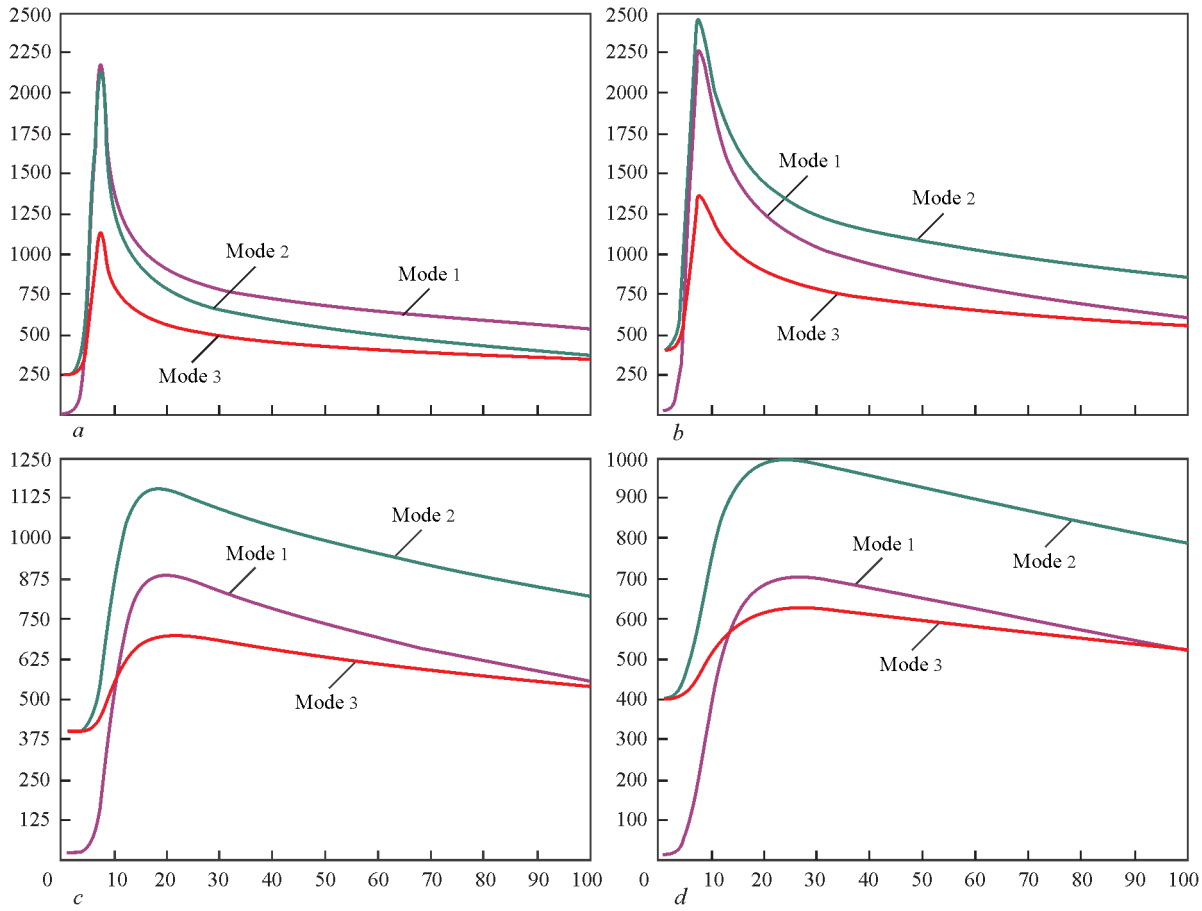

Figure 7. Welding thermal cycles produced by mathematical modeling: *a* — on the surface in the weld center; *b* — in the sample middle in the weld center; *c* — in the specimen middle in the HAZ

Sn–0.6Mo–0.5Nb–0.75Si was performed in OB1826 unit at straight polarity direct current using VDU 511 power source. Specimens were preheated in an electric furnace fitted with heating of shielding gas — argon to protect the welded joint reverse side. Application of an electric furnace with shielding gas heating allowed preheating the samples of high-temperature titanium alloy Ti–6.5Al–5.3Zr–2.2Sn–0.6Mo–0.5Nb –0.75Si up to temperatures of 400 °C.

Welding was performed in modes 1 and 2 (see Table 2), sheet thickness was 6 mm, sample length was 180 mm, and their width was 100 mm. In mode 2 complete penetration of the welded joint of experimental high-temperature titanium alloy Ti–6.5Al–5.3Zr–2.2Sn–0.6Mo–0.5Nb–0.75Si was produced. Experimental thermal cycles were derived using thermocouples of chromel-alumel composition, which were located in point 3 – on the HAZ surface, at 14 mm distance from the weld middle. The derived experimental thermal cycles together with the calculated thermal cycles determined by modeling, are given in Figure 8. As one can see from the Figure, the difference between the experimental and calculated data is equal to 2–5 %.

The diagrams of cooling rate distribution in the temperature range of 600–1200 °C in the welded joint cross-section were plotted as a result of the work performed. It was found that at cooling from 1200 to 1100 °C temperature the cooling rates on the surface in the middle of the weld are higher than 130 °C/s, those in the weld metal lower part and on the boundaries of the weld and the HAZ are equal to 70–130 °C/s, in the rest of the HAZ the metal is cooled at the rate not lower than 31 °C/s (Figure 9, *a*). In the case of application of preheating at 400 °C temperature, at cooling from the temperature of 1200 to 1100 °C the cooling rates on the weld center surface also exceed 130 °C/s, in the weld metal lower part and on the boundaries of

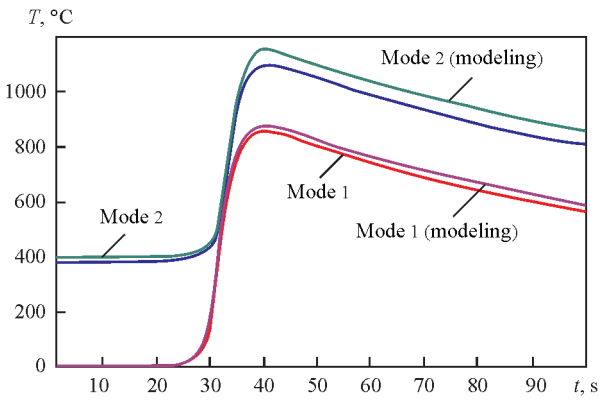

Figure 8. Comparison of experimental and calculated welding thermal cycles

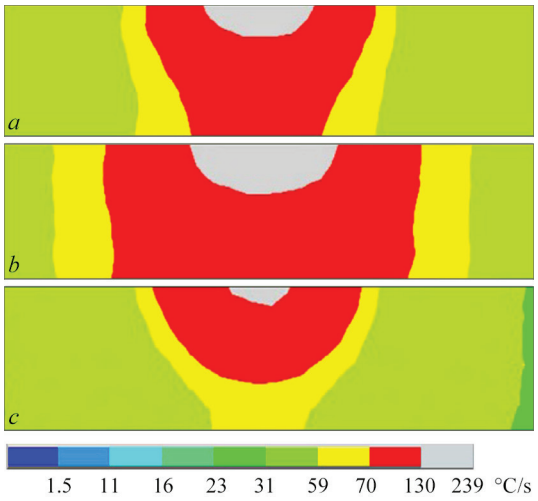

Figure 9. Distribution of cooling rates in the temperature range of 1200–1100 °C: *a* — mode 1; *b* — mode 2; *c* — mode 3

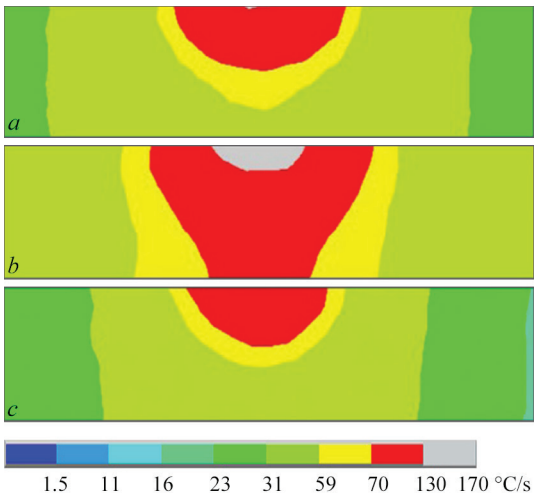

Figure 10. Distribution of cooling rates in the temperature range of 1000–900 °C: *a* — mode 1; *b* — mode 2; *c* — mode 3

the weld and HAZ they are equal to 70–130 °C/s, in the rest of the HAZ the metal is cooled at the rate not lower than 31 °C/s (Figure 9, *b*). Compared to mode 1, in mode 2 the zone with cooling rates higher than 70 °C /s becomes wider.

The mode with lower energy input (Figure 9, *c*) allows reducing the cooling rates by 30–32 % relative to mode 2 and by 35–60 % relative to mode 1 in the entire temperature range.

A similar pattern is observed also in the temperature range of 1000–900 °C (Figure 10, *a*), except that the zone of maximal cooling rates (more than 130 °C/s) is somewhat smaller, but in this zone higher maximal cooling rates are recorded. At application of preheating (mode 2), maximal cooling rates are recorded in the same temperature range in the weld center on the surface and they are equal to 130 °C/s. In the HAZ these values are 59–70 °C/s (Figure 10, *b*). In mode 3 the cooling rates higher than 130 °C/s are not recorded at all in the weld metal (Figure 10, *c*).

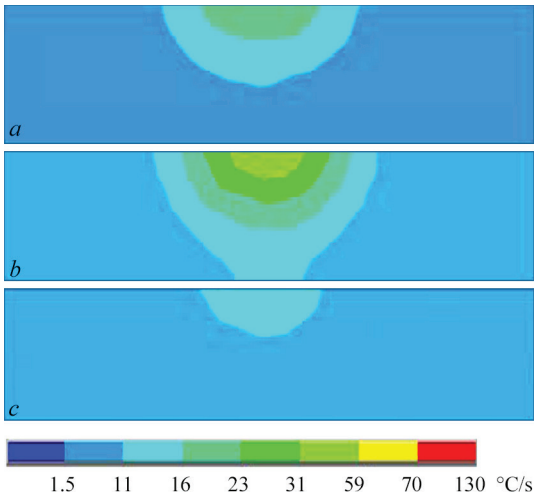

Figure 11. Distribution of cooling rates in the temperature range of 700–600 °C: *a* — mode 1; *b* — mode 2; *c* — mode 3

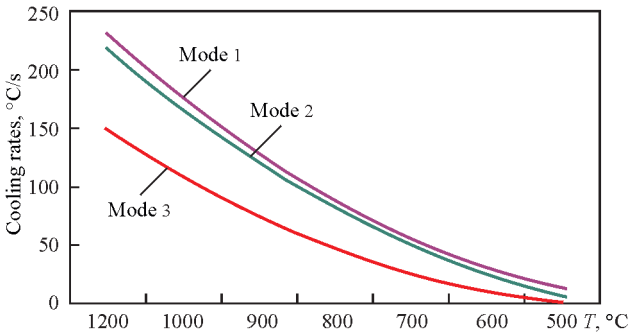

Figure 12. Comparison of cooling rate values

At cooling from the temperature of 700 °C and lower, the cooling rates still remain at a sufficiently high level (120 °C/s in the weld center, 31–70 °C/s in the HAZ) (Figure 11, *a*). Here, the maximal cooling rates in mode 1 have higher values, than in mode 2 with preheating. At cooling from the temperature of 700 °C in mode 2 (Figure 11, *b*), the total range of cooling rates grows noticeably, being equal to 1.5–31 °C/s, compared to the mode without preheating. Mode 3 with smaller energy input and with preheating allows lowering the cooling rates by 35–60 % relative to mode 1 and ensures sample penetration depth of 4.15 mm. Such a penetration depth is achieved in welding in mode 1.

A comparative graph of the dependence of maximal cooling rates on temperatures in the range from 1200 to 500 °C was plotted for points on the surface in the middle of the weld, where the maximal cooling rates are recorded respectively. It was found that in welding 6 mm samples of high-temperature alloy Ti–6.5Al–5.3Zr–2.2Sn–0.6Mo–0.5Nb–0.75Si in mode 2 (with preheating up to 400 °C) the cooling rates are lower than those in mode 1 (without preheating) — by 7–12 % (Figure 12).

CONCLUSIONS

A mathematical model of TIG welding of high-temperature titanium alloy of Ti–6.5Al–5.3Zr–2.2Sn–0.6Mo–0.5Nb–0.75Si system was developed allowing for preheating of the welded joint to 400 °C temperature.

It was found that the heat capacity of experimental high-temperature titanium alloy of Ti–6.5Al–5.3Zr–2.2Sn–0.6Mo–0.5Nb–0.75Si system in the temperature range from 327 to 1127 K, is by 5–7 % higher than that of VT1-00 alloy, and in the temperature range from 1527 to 1860 K it is by 7–10 % lower.

It is shown that application of preheating to the temperature of 400 °C allows increasing the penetration depth of welded joints of high-temperature alloy Ti–6.5Al–5.3Zr–2.2Sn–0.6Mo–0.5Nb–0.75Si by 30 %, the weld width increasing by 17 %.

The plotted distribution of welded joint cooling rates in the temperature range of 500–1200 °C led to the conclusion that the cooling rates in welding with preheating to 400 °C are lower than those in welding without preheating — by 7–12 %, respectively.

References

1. Taranova, T.G., Tunik, A.Yu., Akhonin, S.V. et al. (2012) Peculiarities of structure of Ti–Si–X titanium alloy joints with dispersion hardening performed by electron beam welding. *Visnyk NUK,* **5**, 125–130 [in Ukrainian].
2. Anca, A., Cardona, A., Risso, J., Fachinotti, V.D. (2011) Finite element modeling of welding processes. *Applied Mathematical Modelling*, 35(**2**), 688–707.
3. Akhonin, S.V., Berezos, V.O., Pikulin, O.M. et al. (2022) Producing high-temperature titanium alloys of Ti–Al–Zr–Si–Mo–Nb–Sn system by electron beam melting. *Suchasna Elektrometal.*, **2**, 3–9 [in Ukrainian]. DOI: https://doi.org/10.37434/sem2022.02.01
4. Akhonin, S.V., Severin, A.Yu., Pikulin, O.M. et al. (2022) Structure and mechanical properties of high-temperature titanium alloy of Ti–Al–Zr–Si–Mo–Nb–Sn system after deformation treatment. *Suchasna Elektrometal.*, **4**, 43–48 [in Ukrainian]. DOI: https://doi.org/10.37434/sem2022.04.07
5. Akhonin, S.V., Bilous, V.Yu., Selin, R.V. et al. (2022) Argon-arc welding of high-temperature titanium alloy doped by silicon. *The Paton Welding J.*, **5**, 26–32. DOI: https://doi.org/10.37434/tpwj2022.05.04
6. Akhonin, S.V., Belous, V.Yu., Selin, R.V. (2021) Effect of pre-heating and post-weld local heat treatment on the microstructure and mechanical properties of low-cost β-titanium alloy welding joints, obtained by EBW. *Defect and Diffusion Forum*, **416**, 87–92.
7. Bros, H., Michel, M., Castanet, R. (1994) Enthalpy and heat capacity of titanium based alloys. *J. of Thermal Analysis and Calorimetry*, 41(**1**), 7–24.
8. Maglić, K.D., Pavičić, D.Z. (2001) Thermal and electrical properties of titanium between 300 and 1900 K. *Inter. J. of Thermophysics*, **22**, 1833–1841.
9. Akhonin, S.V., Belous, V.Y., Selin, R.V., Kostin, V.A. (2021) Influence of TIG welding thermal cycle on temperature distribution and phase transformation in low-cost titanium alloy. In: *Proc. of IOP Conf. Series: Earth and Environmental Sci*., 688(**1**), 012012.
10. Akhonin, S.V., Belous, V.Yu., Muzhichenko, A.F., Selin, R.V. (2013) Mathematical modeling of structural transformations in HAZ of titanium alloy VT23 during TIG welding. *The Paton Welding J.*, **3**, 24–27.

ORCID

R.V. Selin: 0000-0002-2990-1131,
V.Yu. Bilous: 0000-0002-0082-8030,
I.B. Selina: 0000-0002-4010-3819

CONFLICT OF INTEREST

The Authors declare no conflict of interest

CORRESPONDING AUTHOR

R.V. Selin
E.O. Paton Electric Welding Institute of the NASU
11 Kazymyr Malevych Str., 03150, Kyiv, Ukraine.
E-mail: selinrv@gmail.com

SUGGESTED CITATION

R.V. Selin, V.Yu. Bilous, S.B. Rukhanskyi, I.B. Selina, L.M. Radchenko (2024) Influence of preheating on TIG welding thermal cycle of high-temperature titanium alloy of Ti–Al–Zr–Sn–Mo–Nb–Si system. *The Paton Welding J.*, **2**, 8–13.

JOURNAL HOME PAGE

https://patonpublishinghouse.com/eng/journals/tpwj

Received: 13.03.2023
Received in revised form: 28.11.2023
Accepted: 29.01.2024